Modeling mechanochemical coupling in cell polarity maintenance

Ondrej Maxian

February 1, 2024

Cell polarity is essential for many aspects of organismal development and physiology, including stem cell dynamics, directional cell migration, and asymmetric cell division [6, 10, 12, 18]. On a large scale, a cell's polarity state is encoded by asymmetric distributions of protein molecules, which are shaped by smaller-scale processes like binding, diffusion, and active transport. The key group of proteins involved in this process are the so-called PAR proteins, which are highly conserved across the metazoa, and are typically distributed asymmetrically during cell division [14, 17] in the presence of actomyosin-mediated contractile flows [21].

The one-cell *C. elegans* embryo is one of the premier model systems for polarization in eukaryotic cells. In this system, polarity is encoded by the distribution of two distinct groups of polarity proteins: anterior PARs (aPARs), which include PAR-3, PAR-6/PKC-3, and CDC-42, and posterior PARs (pPARs), which include PAR-2, PAR-1, LGL-1, and CHIN-1 [17]. Wild-type embryos polarize in two distinct phases termed "establishment" and "maintenance" [3]. In establishment phase, a local sperm cue at the anterior pole acts to load PAR-2 onto the membrane, while at the same time promoting strong anterior-directed actomyosin flows [7]. These cues, together with the mutual inhibition of the aPAR and pPAR domain, sort the PAR proteins into their respective domains, where they are then maintained during maintenance phase [21, 26].

In the language of dynamical systems, it can therefore be said that the *C. elegans* embryo possesses two stable states: a uniform state, in which all of the proteins are distributed symmetrically throughout the cell, and a polarized state, in which the PAR proteins are sorted into their respective domains. The switch between the two states is then governed by the sperm cue, which drives an advective flow to transform the uniform state to the polarized one [9, 11]. Indeed, recent theoretical and experimental studies showed that the cell operates in a regime where cues are necessary to establish polarity, thus avoiding the potentially chaotic case of spontaneous polarization without cues [11].

This analysis suggests that cue-driven flows are required for polarity establishment, and that flow

patterns PAR proteins. Yet, it has been demonstrated repeatedly that embryos lacking a functional flow during establishment phase still polarize, albeit in a delayed manner, and furthermore find the same boundary position as embryos with a functional establishment-phase flow [29, 28]. The flows in these embryos result from a switch from rho-dependent contractility in establishment phase to CDC-42-dependent contractility in maintenance phase [26]. Still though, absent the cue the PAR proteins are the only agents that could pattern actomyosin flows. Thus, these "maintenance-phase" rescue experiments hint that PAR proteins pattern flows, rather than the other way around. This gets at the general question: what are the design principles by which cells combine the PAR protein circuit with actomyosin to robustly encode a dynamically stable polarity state with a fixed boundary position?

Because of the complexity of the *in vivo* system, a definitive answer to this question is only possible with a combination of experiments and modeling. This fact was recognized early on in the field, and indeed there is no dearth of models in the literature (see [27, 5, 4, 8, 11, 9, 15] for a subset). In early models, *potential* mechanics for polarization were explored, but the relative abundance of experimental data in the last decade can allow us to be more precise. For example, an early model of Tostevin and Howard showed that polarity sorting could occur if actomyosin flows feedback onto the aPAR [27] but not pPAR distribution, but recent experiments have shown that both cortical aPARs and pPARs are transported by myosin [13]. We do not take the harsh view that these early models are incorrect; rather, we view them as missing some fundamental biochemistry that was at the time unknown. Consequently, our goal here is to construct a minimal model based on existing experimental evidence that shows how the combination of aPAR/pPAR mutual inhibition and actomyosin flows generate a stable polarity state with fixed boundary position.

Still working on this introductory part. Once we set up a bistable reaction system, the question becomes how we can move from the uniform to the polarized state. Experiments suggest that there are two intrinsic boundary positions here: one (at about 75% egg length) that occurs in the absence of actomyosin flows, and another (at about 50% egg length) that occurs with actomyosin flows [29]. The second case suggests that flows alter the flux balance between the anterior and posterior domains, thus shifting the boundary positions. Indeed, there is a steady state nonzero flow profile observed during maintenance phase, corresponding to an asymmetry in myosin intensity across the A/P boundary [25].

Two questions arise when we consider this data: first, how is the myosin asymmetry maintained without cues? Second, what "brakes" the contractility, i.e., what stops the anterior cap

2

from contracting off the end of the embryo? The first question can be answered again through experiments and modeling, which have shown that PAR proteins feedback onto myosin dynamics [11, 1]. It remains unclear whether this occurs through pPARs inhibiting myosin (as suggested by [1]) or aPARs recruiting myosin (or inhibiting its dissociation, as suggested in [11]). Modeling work has shown that pPARs *must* inhibit myosin to propagate initially asymmetric protein distributions [15]. Seeing as this hypothesis has been supported experimentally [21, 1], it is the one we use in this work.

Once we set up dynamics in which aPARs and pPARs are mutually bistable, and pPARs inhibit myosin, it is straightforward to see how maintenance phase "rescue" could occur, as the already expanding pPAR domain is then further extended by flow caused from inhibited myosin. But how could this process stop? Previous work [9] proposes a "pinning" of the boundary [20] based on cytoplasmic depletion of PAR-2. As the PAR-2 domain expands, the amount available in the cytoplasm decreases. This changes the local binding/unbinding equilibrium, leading to relative depletion of PAR-2 in the posterior. This levels off myosin inhibition levels, which prevents the build up of strong flows, stalling the boundary.

We propose that this mechanism, while theoretically possible and reproducible in our model, is not the one primarily responsible for stalling the boundary movement. Instead, we postulate that branched actin acts to inhibit contractility in the anterior domain, which prevents myosin from building up and generating stronger flows. We demonstrate one of these two things:

1. The hypercontractile state is stable. We can pin it down with the PAR-2 wave-pinning mechanism. The model predicts decreasing PAR-2 on the posterior in this case, which is supported by our experiments.

2. The hypercontractile state is not stable. While we can reproduce it in the model, there is no way to reconcile the parameters we need to reproduce it with the parameters we need to reproduce the wild-type.

Finally, we use modeling to show that branched actin-mediated inhibition of myosin leads to the experimentally-observed myosin and flow profiles, thus validating our hypothesis.

In Section 1, we first rule out the hypothesis that maintenance-phase rescue is driven by spontaneous polarization of myosin, as the flows generated are simply too small to spontaneously polarize the embryo (similar to observations made in establishment phase [22]). We therefore need to incorporate biochemistry to guide the dynamics of myosin. In previous work by some of us [16], we

showed that the maintenance-phase dynamics of PAR-3 are bistable even in the absence of the posterior inhibitor PAR-1. Because of this, it is our hypothesis that PAR-3 provides an anchor for the bistability of the entire system. We utilize this hypothesis in Section 1.2, where we set up a model describing the maintenance phase biochemistry. While this model is capable of amplifying small asymmetries to produce polarized states, the timescale on which this occurs is roughly ten times larger than the duration of maintenance phase, indicating the need for contractility to speed up the process. Therefore, in Section 2, we demonstrate how combining our biochemistry and contractility models can reproduce maintenance-phase experimental observations.

1 Model reveals existing mechanisms cannot explain rescue

1.1 Myosin without additional feedback cannot spontaneously polarize

Movies of the maintenance phase rescue process make it appear as though the system spontaneously breaks symmetry. With that in mind, we explore a possible mechanism whereby the dynamics of myosin could be intrinsically unstable, and those dynamics could generate flows which pattern the PAR proteins. To analyze this, we describe the dynamics of myosin $M(x,t)$ using the advection-diffusion-reaction equations [2]

$$\partial_t M + \partial_x (vM) = D_M \partial_x^2 M + k_M^{\text{on}} M_{\text{cyto}} - k_M^{\text{off}} M \tag{1a}$$

$$\gamma v = \eta \partial_x^2 v + \partial_x \sigma_a(M) \tag{1b}$$

$$M_{\text{cyto}} = \frac{1}{hL} \left(M^{(\text{Tot})} L - \int_0^L M(x) \, dx \right) \tag{1c}$$

The velocity field (1b) comes from the assumption that myosin generates an active stress $\sigma_a(M)$, which combines with the viscous stress to give the total cortical stress $\sigma = \eta \partial_x v + \sigma_a(M)$. As in [2], we ignore the elastic part of the stress, since the actomyosin cortex is purely viscous on timescales longer than the cortical turnover time [19]. The force balance equation in the fluid says that the force due to stress must be balanced by the drag force, $\gamma v = \partial_x \sigma$, where γ is the drag coefficient. Combining the force balance with the stress expression gives the velocity equation (1b).

In the supplemental text, we non-dimensionalize the model equations (1) and reduce the stability analysis to a single dimensionless group $\hat{\sigma}_0 = \frac{\bar{v}}{L k_M^{\text{off}}}$. As $\bar{v}$ represents the typical velocity scale, $1/k_M^{\text{off}}$ represents the time a myosin molecule is bound to the cortex, and L is the embryo perimeter, the dimensionless parameter $\hat{\sigma}_0$ describes the fraction of the embryo perimeter over which a myosin molecule is transported in the time it sits on the cortex.
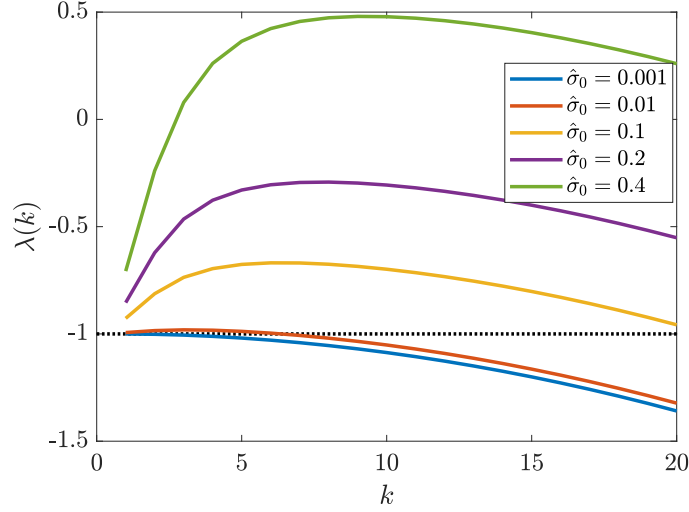
4

Figure 1: Stability analysis for myosin model (1). We consider perturbations of size proportional to $e^{\lambda(k)\hat{t}+2\pi ik\hat{x}}$, then solve the linearized form of (1) to obtain $\lambda(k)$ (see SI). This plot shows $\lambda(k)$ as a function of k and $\hat{\sigma}_0$ (the dimensionless velocity). Positive eigenvalues indicate instability of the steady state. Dotted black line at $\lambda = -1$ reflects the axis of instability *without* unbinding kinetics.

To analyze stability, we introduce a perturbation around the uniform steady state of myosin, $\hat{M} = \hat{M}_0 + \delta\hat{M}$, where $\delta\hat{M} = \delta\hat{M}_0 e^{\lambda(k)\hat{t}+2\pi ik\hat{x}}$, and linearize (1) to solve for the eigenvalue $\lambda(k)$ (see supplemental text). Figure 1 shows the value of $\lambda(k)$ as a function of wavelength k and dimensionless flow speed $\hat{\sigma}_0$. We observe strong flow coupling required for instability; with $\hat{\sigma}_0 = 0.2$ (flow transports myosins around 20% of the cell before they come off), we still do not see any instability. In wild-type embryos, we estimate $\hat{\sigma}_0 \approx 0.03$ (see SI), it is clear that myosin cannot self-polarize in the zygote. As discussed in the SI, in maintenance phase embryos, the main factor working *against* build-up of myosin is the short residence time (about 10 s). Specifically, the advective flow must be strong enough to overcome the local increase in unbinding that happens in areas enriched in myosin. Our data clearly demonstrate that this does not occur in maintenance phase, making the dynamics of myosin by itself stable to perturbations. This means that maintenance-phase rescue must be a result of PAR proteins signaling myosin. The next section lays out our model of the maintenance phase PAR protein circuit that we use for this purpose.

1.2 Basic maintenance-phase biochemistry circuit

Our biochemistry model is based on the diagram shown in Fig. 2, which in turn comes from [17, Fig. 2]. On the anterior side, we have three distinct protein species: PAR-3 (A), CDC-42 (C), and
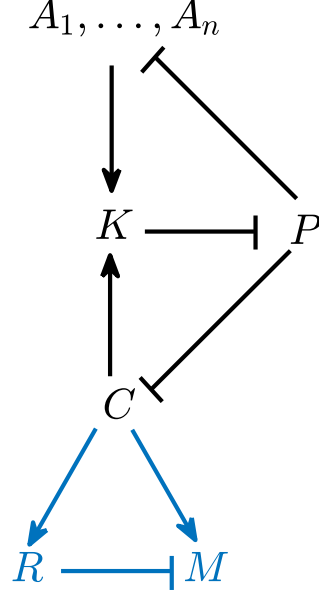
Figure 2: Schematic of the biochemistry model. We consider the black parts (biochemistry only) in Section 1.2, and add the blue parts (contractility) in Section 2. On the anterior half, A represents PAR-3 (in monomer and oligomer form), K represents the PAR-6/PKC-3 complex, and C represents CDC-42. The posterior PARs can be represented by a single protein species P.

PAR-6/PKC-3 (K), each of which has a separate function. The posterior PARs (PAR-2, PAR-1, and CHIN-1) can be lumped into one species (denoted by P), which antagonizes both PAR-3 and CDC-42. The dimensional equations which describe the circuit are

$$\partial_t A_1 = D_A \partial_x^2 A_1 + k_A^{\mathrm{on}} \left(1 + k_A^+ f_A^+(A)\right) A_{\mathrm{cyto}} - k_A^{\mathrm{off}} A_1 \tag{2a}$$

$$+ 2k_A^{\mathrm{dp}}(P)\hat{A}_2 - 2k_A^{\mathrm{p}}\hat{A}_1^{\,2} + \sum_{n=3}^{N} \left(A_n - k_A^{\mathrm{dp}}(P)A_1 A_{n-1}\right)$$

$$\partial_t A_n = k_A^{\mathrm{p}} A_1 (A_{n-1} - A_n) - k_A^{\mathrm{dp}}(P)(A_n - A_{n+1}) \qquad N > n \geq 2 \tag{2b}$$

$$\partial_t A_N = k_A^{\mathrm{p}} A_1 A_{N-1} - k_A^{\mathrm{dp}}(P)A_N \tag{2c}$$

$$\partial_t C = D_C \partial_x^2 C + k_C^{\mathrm{on}} C_{\mathrm{cyto}} - k_C^{\mathrm{off}} \left(1 + r_{\mathrm{PC}} P\right) C \tag{2d}$$

$$\partial_t K = D_K \partial_x^2 K + r_{\mathrm{ACK}} C \delta_{A>A_0} K_{\mathrm{cyto}} - k_K^{\mathrm{off}} K \tag{2e}$$

$$\partial_t P = D_P \partial_x^2 P + k_P^{\mathrm{on}} P_{\mathrm{cyto}} - k_P^{\mathrm{off}} \left(1 + \hat{r}_{\mathrm{KP}} K\right) P \tag{2f}$$

The PAR-3 equations (2a)–(2c) describe the dynamics of PAR-3 oligomerization, for which we use the model developed in [16]. As discussed in detail there, the combination of oligomerization (an oligomer of size n denoted by A_n) and positive feedback (through the term $k_A^+ f_A^+(A)$) imparts intrinsic bistability to the system. This bistability is strengthened when pPARs are included;

through the term $k_A^{\mathrm{dp}}(P)$, these posterior PARs promote depolymerization of PAR-3.

PAR-3 also gates the association of CDC-42 with PAR-6/PKC-3 (K), which is a complex that inhibits all posterior PARs. To model this, we work off the observations in [25], which reveal that PAR-6/PKC-3 are recruited to the membrane by CDC-42, provided that there is a sufficient concentration (roughly 10% of the enriched anterior level) of PAR-3 on the membrane. Absent PAR-3, there is no loading of PAR-6/PKC-3 onto the membrane, so we have no basal rate of loading, and the total loading term in (2e) is proportional to the CDC-42 concentration times the cytoplasmic concentration of K, provided the PAR-3 concentration satisfies $A > A_0$. The other two equations (for CDC-42 and pPARs) are straightforward: we assume a basal rate of binding and unbinding, with an unbinding rate which is linearly enhanced by the inhibitor (pPARs for CDC-42 and PKC-3 for pPARs).

In the supplemental appendix, we nondimensionalize (2), then use sets of existing experimental observations about the relative amount of each species on the anterior/posterior side of the embryo, as well as estimates of the amounts in the cortex vs. cytoplasm, to constrain the parameters.

1.3 The slow journey to a stable boundary position

Update with real times and clean up as it's a little messy right now. In previous work on PAR-3 [16], we demonstrated that the diffusion of the smaller oligomer sizes (monomers in our model) sets a unique boundary position. Because the shift in the boundary is controlled by the slow process of diffusion, it ocurs on timescales of hours, meaning that the boundary never reaches a steady position in practice. In Fig. 3, we demonstrate that this observation still holds when we account for the full biochemistry. In particular, we show the contraction of a PAR-3 domain that initially takes up 90% of the embryo (pPARs are enriched in the other 10%). Initially, the boundary shifts because a high concentration of pPARs shifts the local equilibrium of PAR-3 oligomerization towards the monomer state, which makes bistability impossible [16]. Consequently, we observe contraction of the PAR-3 domain, with a peak that grows over time, and expansion of the PAR-2 domain, both of which eventually reach a steady state.

The concentration of PAR-2 at the edge of the domain decreases over time, which suggests that cytoplasmic depletion might be responsible for halting the boundary, as there is at some point too much A and not enough P for P to win the competition (the decrease in P comes from both cytoplasmic depletion and cytoplasmic enrichment of CDC-42/PAR-6/PKC-3, which inhibit P). To demonstrate that the cytoplasmic dynamics are key to arresting posterior domain expansion, in
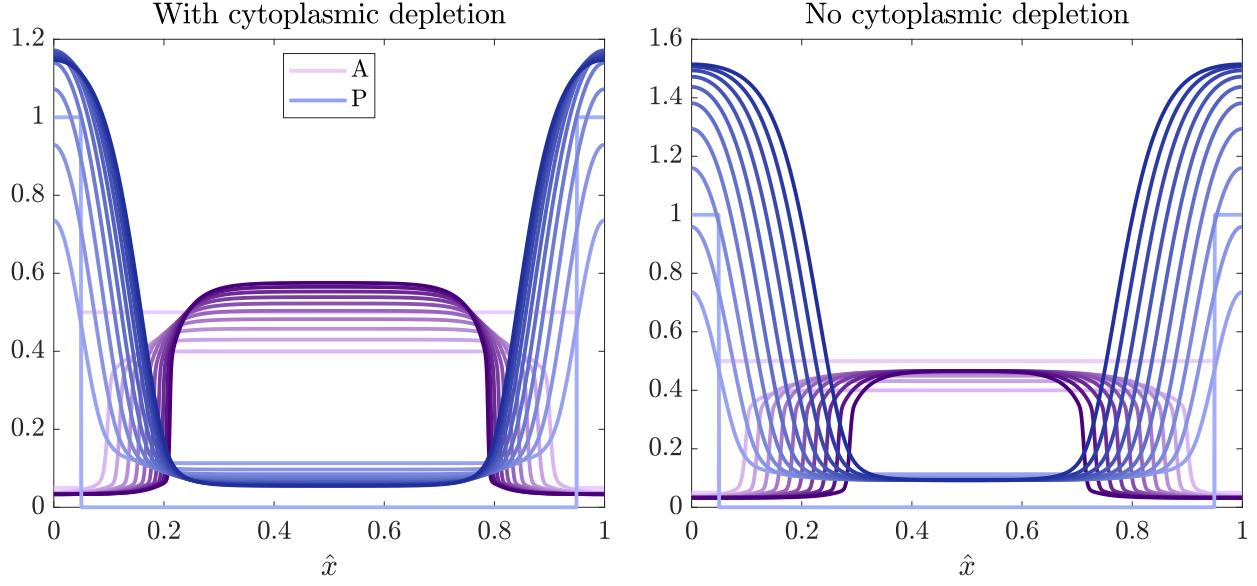
Figure 3: Simulating the biochemistry dynamics (2) with (left) and without (right) cytoplasmic depletion. We show a sequence of 11 time points from $\hat{t} = 0$ (the lightest colors) to $\hat{t} = 500$ (the darkest colors). The left plot shows results with the equations as written, while the right plot removes the cytoplasmic pool updates after $\hat{t} = 50$. For clarity of the plot, we show only PAR-3 in purple and pPARs in blue. UPDATE THIS.

the right panel of Fig. 3 we simulate with a cytoplasmic pool that is "frozen" at its value at $\hat{t} = 50$. The result is an anterior domain which shrinks at a constant rate with constant peak concentration, and a posterior domain which expands at a constant rate with the same concentration at the edge. If given enough time, the posterior domain would invade the entire embryo length.

What about the position of the boundary? Fig. 4 shows that the combination of cytoplasmic depletion and diffusion of PAR-3 monomers set a unique boundary position. Small amounts (10%) of initial PAR-3 enrichment lead to a different boundary position because PAR-3 assumes its intrinsic bistable state while the other proteins are distributed uniformly. Initial PAR-3 domain sizes 20% or larger lead to a single steady state boundary with about 50% PAR-3 enrichment and 25% PAR-2 enrichment. The rest of the domain is where the gradient of PKC-3 is set up.

If we begin with 90% PAR-3 enrichment, Fig. 4 shows that the PAR-3 domain size shrinks to roughly 80% after 5 minutes of real time. Considering that 5 minutes is the duration of maintenance phase, the process by which biochemistry amplifies asymmetries is intrinsically too slow to explain the maintenance-phase rescue process we see in live embryos. In the next section, we couple the contractility of Section 1 to biochemistry to speed up the rescue process.
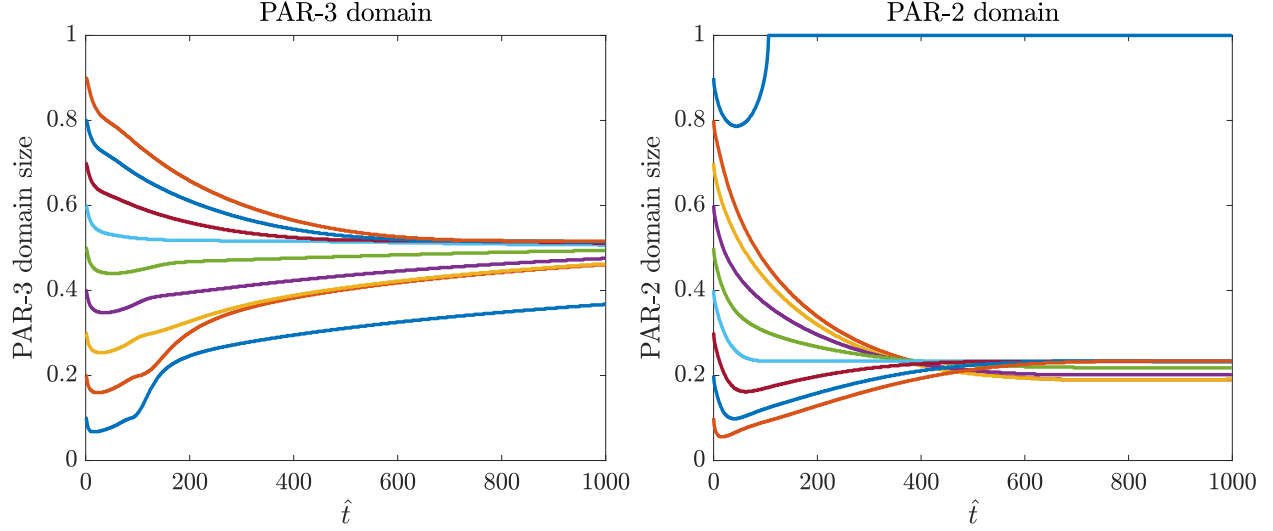
8

Figure 4: Size of the PAR-3 (left) and PAR-2 (right) domain over time for simulations of the model (2). Here the domain size is measured by the length of domain where a particular protein concentration is 80% of its maximum or larger.

2 Coupling contractility to biochemistry

Because myosin cannot form patterns on its own, there must be an interaction with PAR proteins that amplifies gradients in contractility to rescue the correct polarized state. To account for this, we add the myosin dynamics (1) to the biochemistry system (2). In doing this, we also incorporate advective terms that ensure that each protein moves with the local cortical velocity [13], and make CDC-42 a promoter of myosin by adding a term of the form $\hat{R}_{\text{CM}}\hat{C}\hat{M}_{\text{cyto}}$. In dimensionless form,

the coupled system is

$$\partial_{\hat{t}}\hat{A}_1 + \hat{\sigma}_0\partial_{\hat{x}}\left(\hat{v}\hat{A}_1\right) = \hat{D}_A\partial_{\hat{x}}^2 A_1 + \hat{K}_A^{\mathrm{on}}\left(1 + \hat{K}_A^{\mathrm{f}}\hat{F}_A(\hat{A})\right)\left(1 - \int_0^1 \hat{A}(x)\,d\hat{x}\right) - \hat{K}_A^{\mathrm{off}}\hat{A}_1 \tag{3a}$$

$$+ 2\hat{A}_2 - 2\hat{K}_{\mathrm{AP}}^{\mathrm{p}}\hat{A}_1^2 + \sum_{n=3}^N \left(\hat{A}_n - \hat{K}_{\mathrm{AP}}^{\mathrm{p}}\hat{A}_1\hat{A}_{n-1}\right)$$

$$\partial_{\hat{t}}\hat{A}_n + \hat{\sigma}_0\partial_{\hat{x}}\left(\hat{v}\hat{A}_n\right) = \hat{K}_{\mathrm{AP}}^{\mathrm{p}}\hat{A}_1(\hat{A}_{n-1} - \hat{A}_n) - (\hat{A}_n - \hat{A}_{n+1}) \qquad N > n \geq 2 \tag{3b}$$

$$\partial_t\hat{A}_N + \hat{\sigma}_0\partial_{\hat{x}}\left(\hat{v}\hat{A}_N\right) = \hat{K}_{\mathrm{AP}}^{\mathrm{p}}\hat{A}_1\hat{A}_{N-1} - \hat{A}_N \tag{3c}$$

$$\partial_{\hat{t}}\hat{C} + \hat{\sigma}_0\partial_{\hat{x}}\left(\hat{v}\hat{C}\right) = \hat{D}_C\partial_{\hat{x}}^2\hat{C} + \hat{K}_C^{\mathrm{on}}\left(1 - \int_0^1 \hat{C}(\hat{x})\,d\hat{x}\right) - \hat{K}_C^{\mathrm{off}}\left(1 + \hat{R}_{\mathrm{PC}}\hat{P}\right)\hat{C} \tag{3d}$$

$$\partial_{\hat{t}}\hat{K} + \hat{\sigma}_0\partial_{\hat{x}}\left(\hat{v}\hat{K}\right) = \hat{D}_K\partial_{\hat{x}}^2\hat{K} + \hat{R}_{\mathrm{ACK}}\hat{C}\delta_{\hat{A}>\hat{A}_0}\left(1 - \int_0^1 \hat{K}(\hat{x})\,d\hat{x}\right) - \hat{K}_K^{\mathrm{off}}\hat{K} \tag{3e}$$

$$\partial_{\hat{t}}\hat{P} + \hat{\sigma}_0\partial_{\hat{x}}\left(\hat{v}\hat{P}\right) = \hat{D}_P\partial_{\hat{x}}^2\hat{P} + \hat{K}_P^{\mathrm{on}}\left(1 - \int_0^1 \hat{P}(\hat{x})\,d\hat{x}\right) - \hat{K}_P^{\mathrm{off}}\left(1 + \hat{R}_{\mathrm{KP}}\hat{K}\right)\hat{P} \tag{3f}$$

$$\partial_{\hat{t}}\hat{M} + \hat{\sigma}_0\partial_{\hat{x}}\left(\hat{v}\hat{M}\right) = \hat{D}_M\partial_{\hat{x}}^2\hat{M} + \hat{K}_M^{\mathrm{on}}\left(1 + \hat{R}_{\mathrm{CM}}\hat{C}\right)\left(1 - \int_0^1 \hat{M}(x)\,dx\right) - \hat{K}_M^{\mathrm{off}}\hat{M} \tag{3g}$$

$$\hat{v} = \hat{\ell}^2\partial_{\hat{x}}^2 v + \hat{\ell}\partial_{\hat{x}}\hat{\sigma}_a(\hat{M}) \tag{3h}$$

$$R_{\mathrm{CM}} = \frac{r_{\mathrm{CM}}C^{(\mathrm{Tot})}}{k_M^{\mathrm{on}}}, \; \hat{K}_M^{\mathrm{on}} = \frac{k_M^{\mathrm{on}}}{hk_A^{\mathrm{dp}}}, \; \hat{K}_M^{\mathrm{off}} = \frac{k_M^{\mathrm{off}}}{k_A^{\mathrm{dp}}}, \; \hat{\sigma}_0 = \frac{\sigma_0/\sqrt{\eta\gamma}}{Lk_A^{\mathrm{dp}}}, \; \hat{D}_M = \frac{D_M}{k_A^{\mathrm{dp}}L^2}, \; \hat{\ell} = \frac{\sqrt{\eta/\gamma}}{L}. \tag{3i}$$

The last equation (3i) defines the key *new* dimensionless parameters relating to myosin. These differ from (**??**) because we can only non-dimensionalize time by one quantity, and we choose here to stick with the depolymerization time $1/k_A^{\mathrm{dp}}$. Table **??** gives the dimensional quantities σ_0, D_M, and k_M^{off}, from which we obtain $\hat{\sigma}_0$, $\hat{D}_M$, and $\hat{K}_M^{\mathrm{off}}$. This leaves two parameters which control the myosin profile: the basal rate k_M^{on}, and the amount that CDC-42 promotes myosin, $\hat{R}_{\mathrm{CM}}$. In wild-type and *arx-2* (RNAi) embryos, the minimum amount of bound myosin is 0.2. This sets k_M^{on} via $k_M^{\mathrm{on}}/(k_M^{\mathrm{on}} + k_M^{\mathrm{off}}h) \approx 0.2$, giving $k_M^{\mathrm{on}} = 0.3$ μm/s. Our task now is to see if there is a value of $\hat{R}_{\mathrm{CM}}$ which will reproduce maintenance phase rescue.

2.1 First attempt to simulate maintenance-phase rescue

We begin by simulating the model (3) (with parameters in Tables **??**–**??**) with different choices of $\hat{R}_{\mathrm{CM}}$. Two time sequences are shown in Fig. 5 ($\hat{R}_{\mathrm{CM}} = 0.2$) and Fig. 6 ($\hat{R}_{\mathrm{CM}} = 1$). In both cases, the initial dynamics are the same: an initially peaked profile of PAR-2 invades the anterior domain, concentrating anterior PARs in the middle and thereby increasing the concentration of pPARs in the posterior. As a result of this, CDC-42 gets inhibited in the posterior, which gives a gradient of

myosin from posterior to anterior. The gradient of myosin generates a flow which further compacts the anterior domain.

The fundamental difference between Figs. 5 and 6 is the strength of the myosin gradient and the resulting flows. In Fig. 5, the rate at which CDC-42 promotes myosin is only 20% of the basal rate, and as a result the myosin gradient and resulting flow speeds are small. As a result, the boundary slowly contracts and is halted by cytoplasmic depletion of PAR-2 [9], similar to what we see without any flows at all. Figure 6 shows what happens when CDC-42 promotes myosin at 100% of the basal rate. There we see a strong myosin gradient and flow, which eventually focuses the PAR-3 domain into the center of the embryo. In the model, this peak will grow until it is balanced by diffusion (this is not shown in Fig. 6, because PAR-3 levels can reach $\hat{A} = 300$ when the peak keeps contracting).

Thus the model has identified two regimes of behavior, depending on the sensitivity of myosin to the CDC-42 concentration. Roughly speaking, if CDC-42 promotes myosin at a rate much smaller than the basal rate, the cytoplasmic dynamics are sufficient to stop the pPARs from invading too far into the anterior domain. But if CDC-42 promotes myosin at a rate comparable to the basal rate, the dynamics show a rapid concentration of the anterior domain into a peaked profile at the anterior pole. To further probe this behavior, in Fig. 7 we plot the size of the PAR-3 domain over time for four different values of $\hat{R}_{\mathrm{CM}}$, including the case of $\hat{R}_{\mathrm{CM}} = 0$, when there are no flows at all. We see again our two regimes of behavior: rescue can occur by slow diffusion of the boundary aided by flows, with an eventual steady state boundary position, or rapid flows can contract the anterior domain off the edge of the embryo.

The two regimes are most obvious when we look at the flow profiles in the right panel of Fig. 7: in the case when the boundary stops by cytoplasmic depletion (red lines), there is a slow increase in the velocity to a steady value. Alternatively, the velocity grows without bound when the domain contracts off the end of the embryo. Our problem is that neither of these two regimes is consistent with the data, where rescue of polarity occurs with an initially fast flow on the order 5–10 μm/min, followed by a slowing down of the flow and a settling to the steady state boundary position. Indeed, in embryos which lack ect-2 and nop-1 [28], maintenance-phase "rescue" of polarity occurs on timescales of a few minutes, and the aPAR domain goes from roughly 90% embryo length to 70% embryo length in a span of 160 seconds ($\hat{t} = 25.6$) [28, Fig. 7D]. We can replicate this behavior only if we set $\hat{R}_{\mathrm{CM}} = 3$, in which case the PAR-3 domain contracts off the end of the embryo in ten minutes' time. Thus, our model cannot predict a transition to a stable boundary with the flow
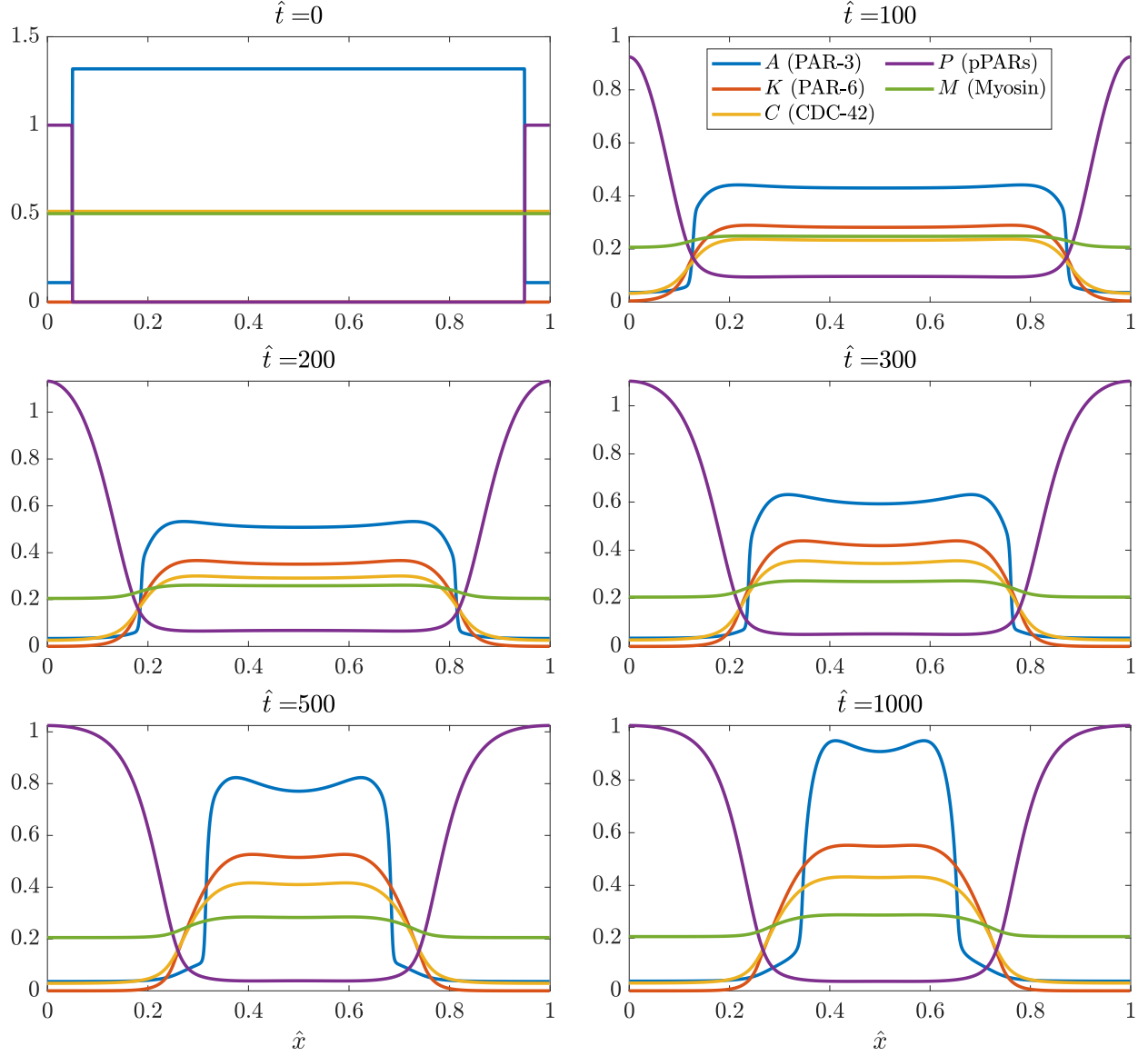
11

Figure 5: Time progression of an initially peaked profile of posterior PARs in the model (3) with $\hat{R}_{\mathrm{CM}} = 0.2$. As shown at $\hat{t} = 0$ at top left, we begin with 10% depletion of PAR-3, then simulate the model (3) with the parameters in Tables **??**–**??**.
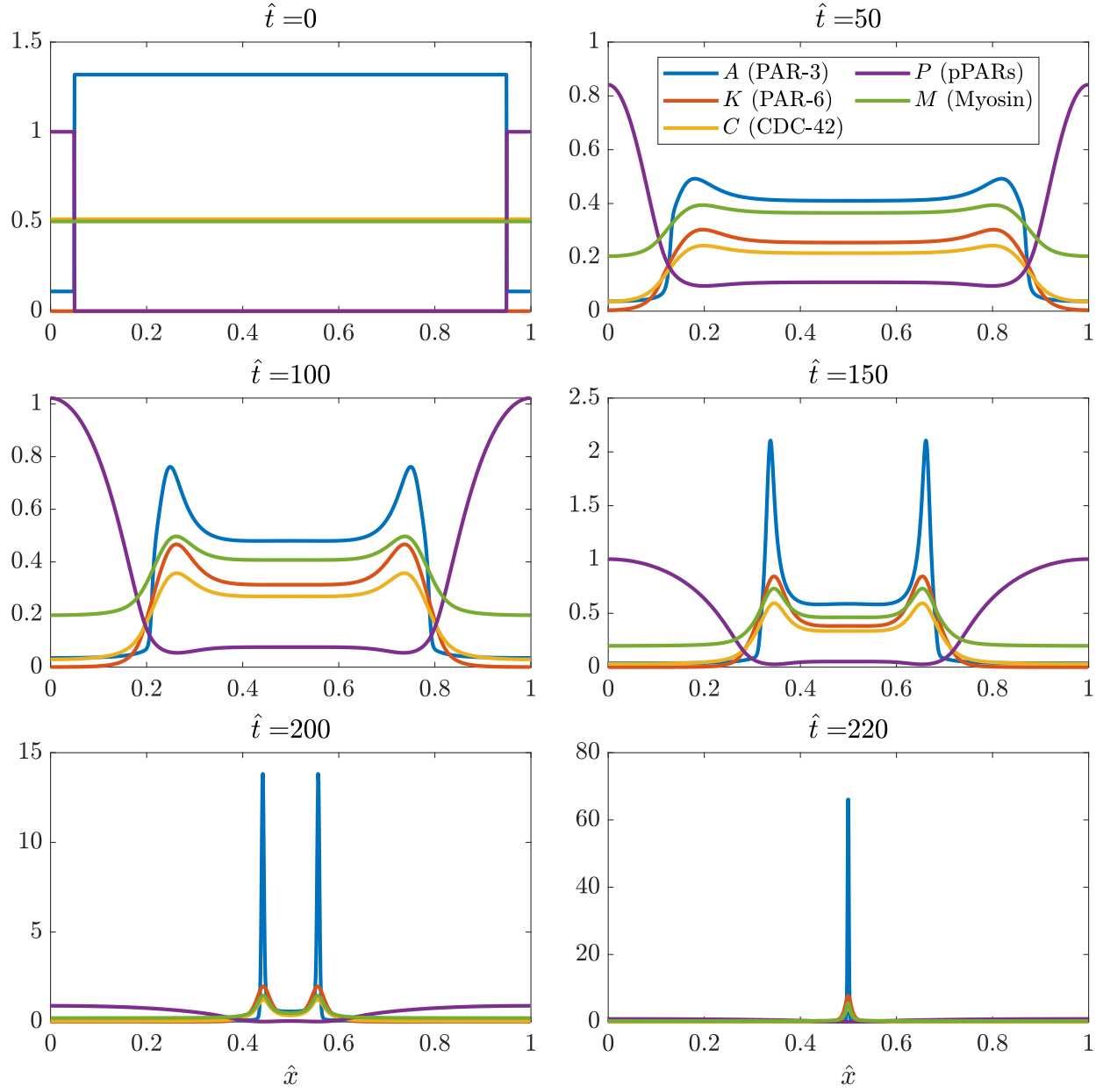
Figure 6: Time progression of an initially peaked profile of posterior PARs in the model (3) with $\hat{R}_{\mathrm{CM}} = 1$.
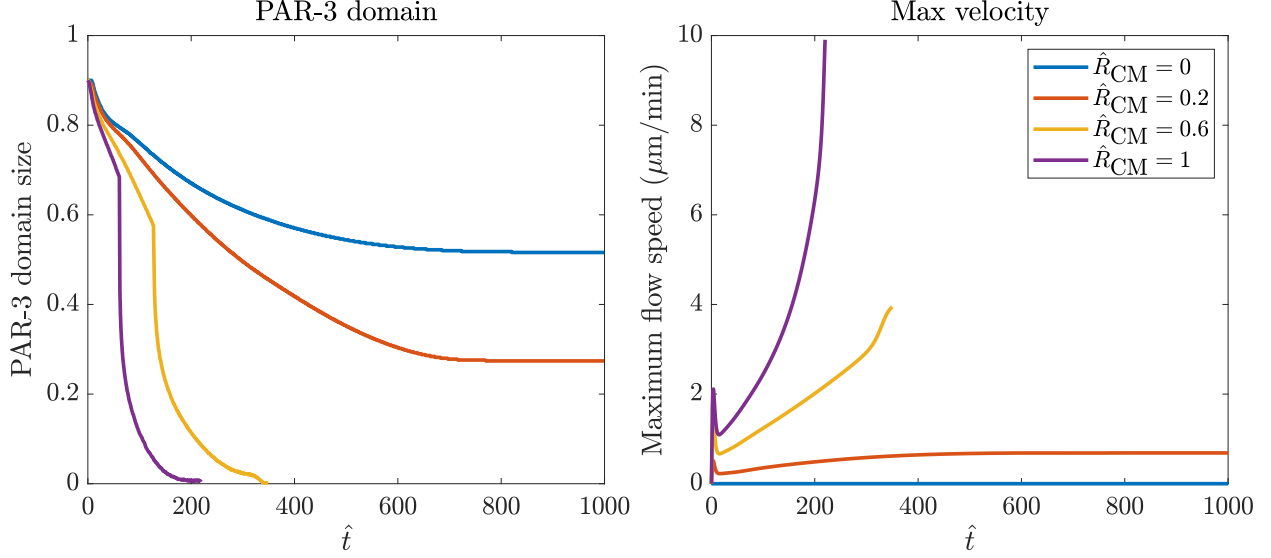
13

Figure 7: Simulations of rescue without branched actin. We repeat the simulation in Fig. 5 with a variety of values of $\hat{R}_{\text{CM}}$ and plot the size of the PAR-3 domain over time (left) and the maximum cortical velocity over time (right).

speeds characteristic of maintenance-phase rescue.

2.2   Incorporating branched actin

The main issue with the models so far is that realistic flow speeds cause the anterior domain to contract off the end of the embryo. So, there must be some mechanism that could counteract the fast flow speeds. Based on our experiments in *arx-2* (RNAi) embryos, which exhibit a hypercontractile state, it seems logical that branched actin could contribute to halting the progression of the anterior domain. Our hypothesis in particular is that branched actin is activated above a certain "threshold" of CDC-42, and that branched actin inhibits contractility by inhibiting myosin. We encode these properties in the system of equations by modifying the myosin equation in (3) and adding an additional equation for branched actin, which we represent by R,

$$\partial_{\hat{t}}\hat{M} + \hat{\sigma}_0 \partial_{\hat{x}}\left(\hat{v}\hat{M}\right) = \hat{D}_M \partial_{\hat{x}}^2 \hat{M} + \hat{K}_M^{\text{on}}\left(1 + \hat{R}_{\text{CM}}\hat{C}\right)\left(1 - \int_0^1 \hat{M}(x)\,dx\right) - \hat{K}_M^{\text{off}}\left(1 + \hat{R}_{\text{RM}}\hat{R}\right)\hat{M}$$

$$\partial_{\hat{t}}\hat{R} + \hat{\sigma}_0 \partial_{\hat{x}}\left(\hat{v}\hat{R}\right) = \hat{D}_R \partial_{\hat{x}}^2 \hat{R} + \hat{R}_{\text{CR}}\left(\hat{C} - \hat{C}_R\right)\delta_{\hat{C} > \hat{C}_R}\left(1 - \int_0^1 \hat{R}(x)\,dx\right) - \hat{K}_R^{\text{off}}\hat{R} \qquad (4)$$

Here branched actin is produced above a threshold level $\hat{C}_R$ of CDC-42, as indicated by the δ-function. Once produced, branched actin inhibits myosin. We assume for the moment that branched actin has the same diffusivity ($0.05\ \mu\text{m}^2/\text{s}$) and unbinding rate ($0.12/\text{s}$) as myosin.

14

Parameter	Description	Value	Units	Ref	Notes
D_R	Branched actin diffusivity	0.05	$\mu m^2/s$		Same as myosin
k_R^{off}	Branched actin unbinding rate	0.12	1/s		Same as myosin
$\hat{R}_{CM}$	C promoting M	3		[28, Fig. 7D]	Fit initial rescue speed
$\hat{C}_R$	Threshold CDC-42 level for branched actin	0.2			Between A and P levels
$\hat{R}_{CR}$	CDC-42 producing branched actin rate	1			Arbitrary
$\hat{R}_{RM}$	Branched actin inhibiting myosin rate	15			Fit boundary position

Table 1: Additional parameters for coupled model (3) with branched actin additions in (4).

2.2.1 Additional parameters

There are four new parameters in this model that are unknown:

- $\hat{R}_{CM}$, which is the rate at which CDC-42 produces myosin. As mentioned in the last section, the value $\hat{R}_{CM} = 3$ gives a good match to the initial speeds of maintenance phase rescue reported in [28, Fig. 7D], which presumably do not yet have interference from branched actin.

- The threshold $\hat{C}_R$ is set by examining the steady state in Fig. 5 without branched actin. There we see that, at late times, CDC-42 goes from about 0.05 in the posterior to 0.45 in the anterior. To block contractility, we set $\hat{C}_R = 0.2$.

- The rate at which CDC-42 produces branched actin sets the amount of bound branched actin. This amount is arbitrary, since what matters is not the amount of branched actin but the total amount of myosin inhibition. We therefore set $\hat{R}_{CR} = 1$.

- We set the rate at which branched actin blocks myosin $\hat{R}_{RM} = 10$, which is the parameter we use to control the dynamics, to reproduce the boundary position in wild type embryos.

The parameters are summarized in Table 1.

2.2.2 Dynamics

Figure 8 shows the dynamics of the approach to steady state for (3) augmented with the branched actin model (4). We see initially the same dynamics as in Fig. 6, with pPARs inhibiting CDC-42 and myosin, which produces an inward flow. However, once the CDC-42 concentration (yellow) gets high enough, branched actin (cyan) starts to be produced and inhibit contractility. This makes the myosin profile decrease, and stalls flow and movement of the boundary. The steady state is
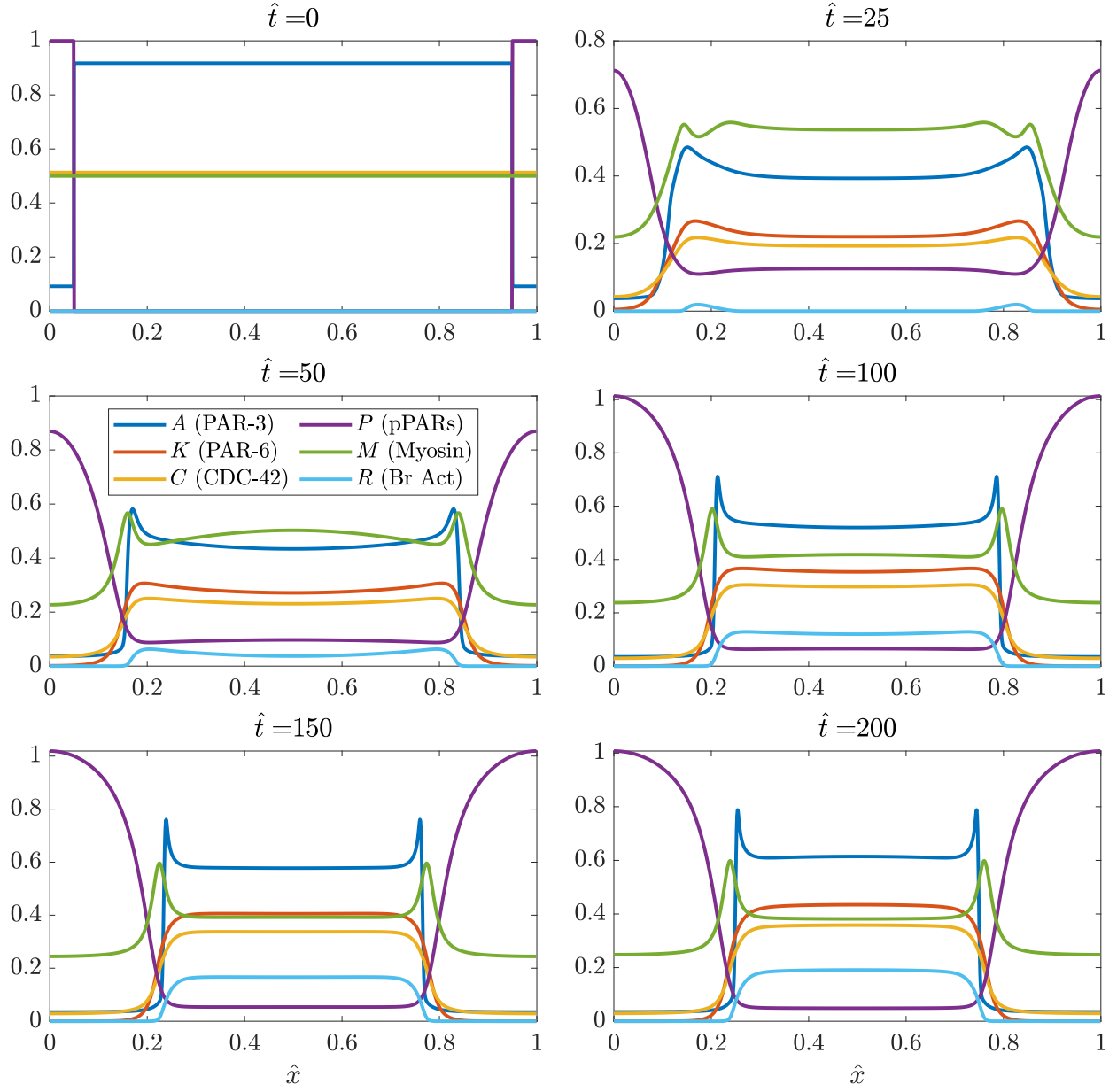
Figure 8: Simulation of maintenance phase rescue with branched actin. As shown at $\hat{t} = 0$ at the top left, we begin with 10% depletion of PAR-3, then simulate the model (3) *with branched actin* as in (4). The size of the aPAR domain initially shrinks rapidly, and then stalls as branched actin (cyan) starts to inhibit contractility.
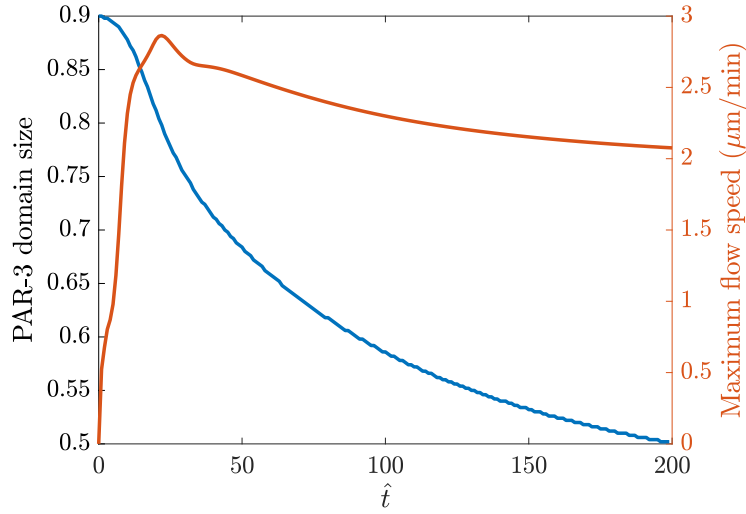
Figure 9: PAR-3 domain size and maximum flow speed in simulations maintenance-phase rescue. The initial conditions are as in the top left Fig. 8, with 90% of the domain enriched in PAR-3. The blue line (left axis) shows the boundary position over time, while the red line (right axis) shows the maximum flow velocity.

reached at about $\hat{t} = 100$, which corresponds to 10 minutes of real time (there is slow contraction of the boundary to its final resting place after this).

The advantage of incorporating branched actin is that we can essentially have arbitrarily fast initial flow speeds, which are later blocked by branched actin. As shown in Fig. 9, in our simulation there is initially a rapid build-up of flow and shrinking of the PAR-3 boundary. The flow then becomes smaller once branched actin kicks in, and both the flow speed and domain size plateau to a steady state. These data for velocity over time qualitatively match what we see in experiments.

There is still a role for cytoplasmic depletion in pinning the boundary. Without cytoplasmic depletion, a boundary that is moving will always keep moving, since the fundamental balance in which pPARs outcompete the aPARs does not change unless we account for changes in the cytoplasmic depletion. What branched actin allows for is a change in how the flow speed depends on the myosin concentration in time. Initially, when there is no branched actin, flows are fast. But, when branched actin is created, the flows slow down and the boundary can no longer rapidly contract, allowing it to be stalled by cytoplasmic depletion. Thus, branched actin *and* cytoplasmic depletion work together to stall the boundary at a point where the posterior PAR domain can no longer advance through the anterior PARs.
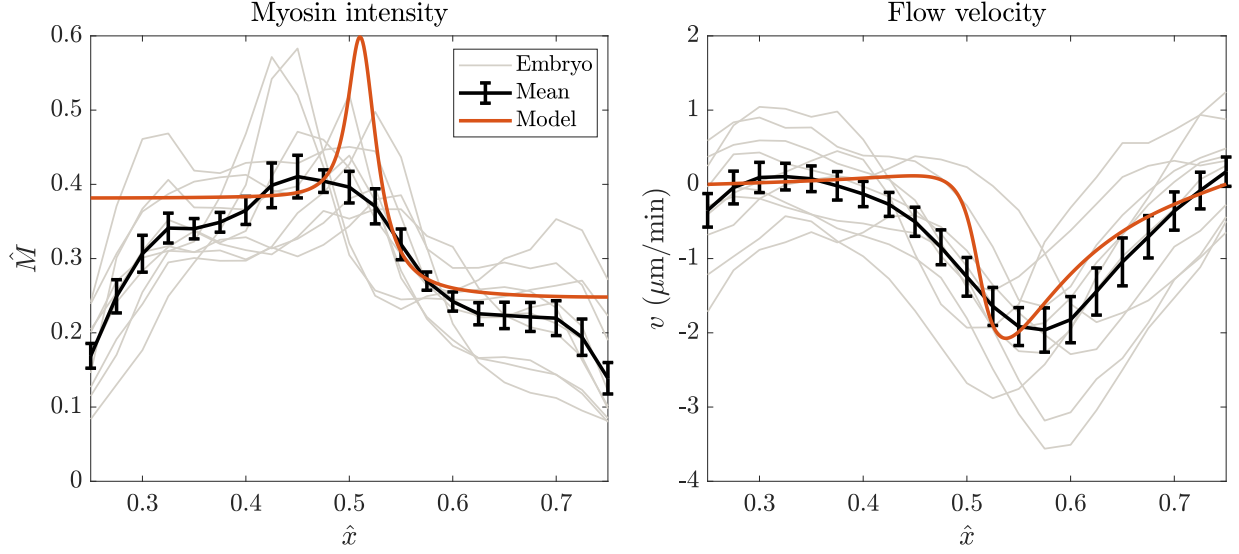
Figure 10: Steady state of the model (3) with branched actin model (4) (this corresponds to $\hat{t} = 200$ in the simulation of maintenance phase rescue depicted in Fig. 8), compared to experimental results for wild-type embryos. The left panel shows the myosin intensity profile, while the right panel shows the speed of flow. Individual embryos are shown using gray lines, the mean $\pm$ standard error are shoiwn in black. Results of the model (shifting the anterior pole to $\hat{x} = 0.25$) are ovelaid in red.

2.2.3 Steady state vs. experiments

Figure 10 shows how our modeled steady state (after $\hat{t} = 200$ of maintenance phase rescue) compares to wild-type embryos (the "steady state" measured in late maintenance phase). Qualitatively, the results match: the myosin intensity displays a peak at the anterior cap, then drops off to a level midway between the peak anterior and posterior levels at the anterior pole. The flow also exhibits a maximum off of the anterior cap, then rapidly transitions to a stall point at the edge of the anterior domain.

Quantitatively, our results almost match up with the experiments, but leave a little to be desired. The issue is the lengthscale on which the drop in myosin occurs. Because branched actin is only active on the anterior cap, the lengthscale on which it goes from zero to its peak value is quite small (controlled by the diffusivity, which here is set equal to the diffusivity of myosin). As such, the myosin is inhibited quickly in the model, and the profile rapidly drops to a flat level in the anterior. This is *not* what is observed in experiments, where we see a more gradual decrease (although the individual embryos do show rapid decreases).

18

References

[1] Alexander Beatty, Diane G Morton, and Kenneth Kemphues. Par-2, lgl-1 and the cdc-42 gap chin-1 act in distinct pathways to maintain polarity in the c. elegans embryo. *Development*, 140(9):2005–2014, 2013.

[2] Justin S Bois, Frank Jülicher, and Stephan W Grill. Pattern formation in active fluids. *Biophysical Journal*, 100(3):445a, 2011.

[3] Adrian A Cuenca, Aaron Schetter, Donato Aceto, Kenneth Kemphues, and Geraldine Seydoux. Polarization of the c. elegans zygote proceeds via distinct establishment and maintenance phases. 2003.

[4] Adriana T Dawes and David Iron. Cortical geometry may influence placement of interface between par protein domains in early caenorhabditis elegans embryos. *Journal of theoretical biology*, 333:27–37, 2013.

[5] Adriana T Dawes and Edwin M Munro. Par-3 oligomerization may provide an actin-independent mechanism to maintain distinct par protein domains in the early caenorhabditis elegans embryo. *Biophysical journal*, 101(6):1412–1422, 2011.

[6] Evan B Dewey, Danielle T Taylor, and Christopher A Johnston. Cell fate decision making through oriented cell division. *Journal of developmental biology*, 3(4):129–157, 2015.

[7] Wan Jun Gan and Fumio Motegi. Mechanochemical control of symmetry breaking in the caenorhabditis elegans zygote. *Frontiers in Cell and Developmental Biology*, 8:619869, 2021.

[8] Raphaela Geßele, Jacob Halatek, Laeschkir Würthner, and Erwin Frey. Geometric cues stabilise long-axis polarisation of par protein patterns in c. elegans. *Nature communications*, 11(1):539, 2020.

[9] Nathan W Goehring, Philipp Khuc Trong, Justin S Bois, Debanjan Chowdhury, Ernesto M Nicola, Anthony A Hyman, and Stephan W Grill. Polarization of par proteins by advective triggering of a pattern-forming system. *Science*, 334(6059):1137–1141, 2011.

[10] Bob Goldstein and Ian G Macara. The par proteins: fundamental players in animal cell polarization. *Developmental cell*, 13(5):609–622, 2007.

[11] Peter Gross, K Vijay Kumar, Nathan W Goehring, Justin S Bois, Carsten Hoege, Frank Jülicher, and Stephan W Grill. Guiding self-organized pattern formation in cell polarity establishment. *Nature physics*, 15(3):293–300, 2019.

[12] Niv Ierushalmi and Kinneret Keren. Cytoskeletal symmetry breaking in animal cells. *Current Opinion in Cell Biology*, 72:91–99, 2021.

[13] Rukshala Illukkumbura, Nisha Hirani, Joana Borrego-Pinto, Tom Bland, KangBo Ng, Lars Hubatsch, Jessica McQuade, Robert G Endres, and Nathan W Goehring. Design principles for selective polarization of par proteins by cortical flows. *Journal of Cell Biology*, 222(8), 2023.

[14] Kenneth J Kemphues, James R Priess, Diane G Morton, and Niansheng Cheng. Identification of genes required for cytoplasmic localization in early c. elegans embryos. *Cell*, 52(3):311–320, 1988.

[15] Natalia Kravtsova and Adriana T Dawes. Actomyosin regulation and symmetry breaking in a model of polarization in the early caenorhabditis elegans embryo: symmetry breaking in cell polarization. *Bulletin of mathematical biology*, 76:2426–2448, 2014.

[16] Charles F Lang, Alexander Anneken, and Edwin Munro. Oligomerization and feedback on membrane recruitment stabilize par-3 asymmetries in c. elegans zygotes. *bioRxiv*, pages 2023–08, 2023.

[17] Charles F Lang and Edwin Munro. The par proteins: from molecular circuits to dynamic self-stabilizing cell polarity. *Development*, 144(19):3405–3416, 2017.

[18] Jean-Léon Maître, Hervé Turlier, Rukshala Illukkumbura, Björn Eismann, Ritsuya Niwayama, François Nédélec, and Takashi Hiiragi. Asymmetric division of contractile domains couples cell positioning and fate specification. *Nature*, 536(7616):344–348, 2016.

[19] Mirjam Mayer, Martin Depken, Justin S Bois, Frank Jülicher, and Stephan W Grill. Anisotropies in cortical tension reveal the physical basis of polarizing cortical flows. *Nature*, 467(7315):617–621, 2010.

[20] Yoichiro Mori, Alexandra Jilkine, and Leah Edelstein-Keshet. Wave-pinning and cell polarity from a bistable reaction-diffusion system. *Biophysical journal*, 94(9):3684–3697, 2008.

[21] Edwin Munro, Jeremy Nance, and James R Priess. Cortical flows powered by asymmetrical contraction transport par proteins to establish and maintain anterior-posterior polarity in the early c. elegans embryo. *Developmental cell*, 7(3):413–424, 2004.

[22] Masatoshi Nishikawa, Sundar Ram Naganathan, Frank Jülicher, and Stephan W Grill. Controlling contractile instabilities in the actomyosin cortex. *Elife*, 6:e19595, 2017.

[23] François B Robin, William M McFadden, Baixue Yao, and Edwin M Munro. Single-molecule analysis of cell surface dynamics in caenorhabditis elegans embryos. *Nature methods*, 11(6):677–682, 2014.

[24] Arnab Saha, Masatoshi Nishikawa, Martin Behrndt, Carl-Philipp Heisenberg, Frank Jülicher, and Stephan W Grill. Determining physical properties of the cell cortex. *Biophysical journal*, 110(6):1421–1429, 2016.

[25] Anne Sailer, Alexander Anneken, Younan Li, Sam Lee, and Edwin Munro. Dynamic opposition of clustered proteins stabilizes cortical polarity in the c. elegans zygote. *Developmental cell*, 35(1):131–142, 2015.

[26] Stephanie Schonegg and Anthony A Hyman. Cdc-42 and rho-1 coordinate acto-myosin contractility and par protein localization during polarity establishment in c. elegans embryos. 2006.

[27] Filipe Tostevin and Martin Howard. Modeling the establishment of par protein polarity in the one-cell c. elegans embryo. *Biophysical journal*, 95(10):4512–4522, 2008.

[28] Yu Chung Tse, Michael Werner, Katrina M Longhini, Jean-Claude Labbe, Bob Goldstein, and Michael Glotzer. Rhoa activation during polarization and cytokinesis of the early caenorhabditis elegans embryo is differentially dependent on nop-1 and cyk-4. *Molecular biology of the cell*, 23(20):4020–4031, 2012.

[29] Seth Zonies, Fumio Motegi, Yingsong Hao, and Geraldine Seydoux. Symmetry breaking and polarization of the c. elegans zygote by the polarity protein par-2. *Development*, 137(10):1669–1677, 2010.